How precipitation intermittency sets an optimal sampling distance for temperature reconstructions from Antarctic ice cores

Thomas Münch[1], Martin Werner[2], and Thomas Laepple[1,3]

[1]Alfred-Wegener-Institut Helmholtz-Zentrum für Polar- und Meeresforschung, Research Unit Potsdam, Telegrafenberg A45, 14473 Potsdam, Germany
[2]Alfred-Wegener-Institut Helmholtz-Zentrum für Polar- und Meeresforschung, Bussestraße 24, 27570 Bremerhaven, Germany
[3]University of Bremen, MARUM – Center for Marine Environmental Sciences and Faculty of Geosciences, 28334 Bremen, Germany

Correspondence: Thomas Münch (thomas.muench@awi.de)

Abstract. Many palaeoclimate proxies share one challenging property: they are not only driven by the climatic variable of interest, e.g., temperature, but they are also influenced by secondary effects which cause, among other things, increased variability, frequently termed *noise*. Noise in individual proxy records can be reduced by averaging the records, but the effectiveness of this approach depends on the correlation of the noise between the records and therefore on the spatial scales of the noise-generating
5 processes. Here, we review and apply this concept in the context of Antarctic ice-core isotope records to determine which core locations are best suited to reconstruct local-to-regional-scale temperatures. Using data from a past-millennium climate model simulation equipped with stable isotope diagnostics we intriguingly find that even for a local temperature reconstruction the optimal sampling strategy is to combine a local ice core with a more distant core ~ 500–1000 km away. A similarly large distance between cores is also optimal for reconstructions that average more than two isotope records. We show that these findings
10 result from the interplay of the two spatial scales of the correlation structures associated with the temperature field and with the noise generated by precipitation intermittency. Our study helps to maximise the usability of existing Antarctic ice cores and to optimally plan future drilling campaigns. It also broadens our knowledge on the processes that shape the isotopic record and their typical correlation scales. Finally, the presented method can be directly extended to determine optimal sampling strategies for other palaeoclimate reconstruction problems.

1 Introduction

The oxygen and hydrogen isotopic composition of firn and ice recovered from polar ice cores is a key proxy for past near-surface atmospheric temperature changes (Dansgaard, 1964; Lorius et al., 1969; Masson-Delmotte et al., 2008; Sjolte et al., 2011). Although the physical mechanisms that link local changes in temperature to the isotopic composition of precipitated snow are generally well understood (Dansgaard, 1964; Craig and Gordon, 1965; Jouzel and Merlivat, 1984) and can be mod-
20 elled with general circulation models (Joussaume et al., 1984; Werner et al., 2011, 2016; Sjolte et al., 2011; Goursaud et al.,

2018), the quantitative interpretation of ice-core isotope variability, in terms of temperature variability, is complicated by second-order processes that influence the isotopic record, adding noise (Münch and Laepple, 2018).

Specifically, the isotopic record that is derived from an ice core is the result of a chain of processes: (1) atmospheric temperature changes along with (2) isotopic fractionation during the pathway from atmospheric moisture to precipitation, (3) the

25   effect of variable and intermittent precipitation and finally (4) local depositional and post-depositional effects. As we outline in the following, each element of this chain can be associated with a typical spatial length scale over which it is correlated.

Atmospheric temperature variations drive the isotopic composition fractionation of the atmospheric moisture along its pathway to the final stage of precipitation (Dansgaard, 1964; Jouzel and Merlivat, 1984). The spatial coherence of the temperature-related isotopic signal in precipitation is hence determined by the spatial coherence of the variations of the atmospheric tem-

30   perature field itself. Typical spatial decorrelation scales for temperature anomalies are on the order of $\gtrsim 1000\,\text{km}$ (Jones et al., 1997), which implies that ice cores distributed on spatial scales below $\sim 1000\,\text{km}$ should typically record a similar, i.e., correlated, temperature signal. However, the temporal variability of the isotopic composition in the local atmospheric moisture also depends on the variability of the atmospheric circulation, since different air masses may exhibit different source regions and distillation pathways (Schlosser et al., 2004; Sodemann et al., 2008; Birks and Edwards, 2009; Küttel et al., 2012). In

35   addition, the isotopic composition profile across a deposited layer of snow will not directly reflect the temporal variability of the atmospheric isotopic signal due to the intermittent nature of precipitation (Schleiss and Smith, 2015). By this, the initial isotope signal is weighted with the amount of precipitation, which introduces bias (Steig et al., 1994; Laepple et al., 2011) and adds additional variability to the isotopic record (Persson et al., 2011; Casado et al., 2020). The latter two processes are linked to atmospheric dynamics and their typical spatial scales range from the mesoscale (i.e., tens of kilometres), driven by topogra-

40   phy and orographic effects, to synoptic scales of hundreds of kilometres, associated with cyclonic activity and the movement of high and low pressure systems. Finally, in polar conditions, the precipitated snow does not directly settle but is constantly eroded, blown away, and redeposited. These depositional processes have been shown to give rise to stratigraphic noise in the isotopic record (Fisher et al., 1985; Münch et al., 2016; Laepple et al., 2016), which exhibits a small-scale decorrelation scale of a few metres (Münch et al., 2016). We note that the final isotopic record is also influenced by potential exchange processes at

45   the surface and by densification and diffusion within the snow and ice, which are, however, not within the scope of this article.

The hierarchy of the different spatial scales of the processes influencing an isotope record determines the effectiveness of reducing the overall noise, since a reduction in the noise level by averaging records will depend on the spatial correlation scale of the different noise sources. For example, if an isotope record were only shaped by temperature variations and stratigraphic noise, it would be sufficient to average records spaced only tens of metres apart, as this would ensure highly correlated temper-

50   ature signals but uncorrelated stratigraphic noise between the records. However, comparing correlation-based signal-to-noise ratios derived from nearby isotope records (Münch et al., 2016, 2017) with the signal-to-noise ratios estimated from analysing the records' temporal variability (Laepple et al., 2018) shows that reproducibility on a local scale does not necessarily imply a climatic, i.e., temperature-driven, origin. Instead, circulation variability and precipitation intermittency act as additional noise sources which are likely to exhibit larger decorrelation lengths than the stratigraphic noise (Laepple et al., 2018; Münch and Laepple, 2018). Taking this into account, we expect there to be an optimal length scale, which lies in between the local

55

and the temperature decorrelation scales and which results in a trade-off between averaging out atmospheric circulation and precipitation intermittency effects, while also ensuring a sufficient coherence in the recorded temperature signal.

The aim of the present study is to use data from a climate model equipped with stable isotope diagnostics to systematically study the different typical process scales – including those from atmospheric temperature variations, circulation variability, precipitation intermittency and the isotope–temperature relationship –, to determine the optimal spatial arrangement of ice-core locations, which maximises the correlation with temperature at a specific target site. To address this problem we focus on target sites on the East Antarctic Plateau. Our results show that the average of multiple ice-core isotope records yields a higher degree of correlation with temperature when the sampled locations are spread across distances of $1000\,\mathrm{km}$ or more from the target site, than when they are all located close ($< 250\,\mathrm{km}$) to the target site. While these results may seem counterintuitive at first, we qualitatively explain their general features with a simple analytical model that uses the typical spatial correlation structures associated with the temperature and isotope fields, and with the noise generated by precipitation intermittency.

2 Data and methods

2.1 Climate model data

We use data from the past-millennium simulation (800–1999 CE; Sjolte et al., 2018) of the fully coupled ECHAM5/MPI-OM-wiso atmosphere–ocean general circulation model equipped with stable isotope diagnostics (Werner et al., 2016). This simulation is forced by greenhouse gases, volcanic aerosols, total solar irradiance, land use changes, and changes in the Earth's orbital parameters. The model's atmospheric component ECHAM5-wiso is run with a T31 spectral resolution ($3.75° \times 3.75°$) and with 19 vertical levels (Sjolte et al., 2018). Compared to observations, the climatological relationship between temperature and the precipitation isotopic composition is reproduced well by the model, but it is biased towards warm temperatures in the T31 setup and its isotopic composition is not depleted enough over Antarctica (Werner et al., 2011). These issues can be improved upon by using a higher spatial resolution (Werner et al., 2011); however, such a higher-resolution model is not needed for our study, since we are mainly interested in the relative variability between sites and not in the absolute temperature or isotope values. The full atmosphere–ocean model was compared to observational data and palaeoclimate records for two equilibrium simulations under pre-industrial and Last Glacial Maximum conditions (Werner et al., 2016), and the past-millennium simulation was used to reconstruct North Atlantic atmospheric circulation in combination with ice-core isotope data (Sjolte et al., 2018).

In this study, we use the 1200-year ECHAM5/MPI-OM-wiso time series of two-metre surface air temperature ($T_{2\mathrm{m}}$), precipitation (p), and oxygen isotopic composition in precipitation (the relative abundance of oxygen-18 to oxygen-16 istopes, denoted as $\delta^{18}\mathrm{O}$) extracted from all $N_{\mathrm{grid}} = 442$ model grid cells on the Antarctic continent (Münch and Werner, 2020).

2.2 Data processing

The model simulation output has a monthly temporal resolution, while typically ice-core isotope records exhibit an annual (or even lower) resolution. The latter is commonly achieved by averaging the isotopic data across annual layers of snow and ice, which are determined through a dating approach. The resulting annual isotopic composition data therefore include a weighting effect due to the intra-annual variability in the amount of precipitation. To account for this, we produce two versions of annual data from the monthly model output (Münch and Werner, 2020): (1) the two-metre temperature and oxygen isotopic composition data are averaged to an annual resolution without any weighting (denoted as $T_{2\mathrm{m}}$ and $\delta^{18}\mathrm{O}$ in the following), and (2) the respective monthly data are averaged to an annual resolution including the weighting by the monthly precipitation amount (denoted as precipitation-weighted data $T_{2\mathrm{m}}^{(\mathrm{pw})}$ and $\delta^{18}\mathrm{O}^{(\mathrm{pw})}$).

2.3 Data analyses

2.3.1 General approach

We investigate the relationships among the model variables by assessing the Pearson correlation coefficient (r). To derive implications for actual ice-core studies, we use the $\delta^{18}\mathrm{O}^{(\mathrm{pw})}$ time series at the model grid cells as a surrogate for ice-core isotope records. We thus neglect stratigraphic noise and any further depositional or post-depositional effects on the isotopic record, since we are interested in the upper limit of the extent to which ice cores can reconstruct the climatic temperature signal in the atmosphere. Our analyses are conducted relative to specified grid cells of interest (target sites; $\mathbf{r}_0$) to obtain results that are relevant on local-to-regional spatial scales.

2.3.2 Picking optimal sites

To determine an optimal set of ice-core locations to reconstruct $T_{2\mathrm{m}}$ at a given target site we first randomly pick without replacement a number N of the grid cells that lie within a circle of $2000\,\mathrm{km}$ radius around the target site and then correlate the average $\delta^{18}\mathrm{O}^{(\mathrm{pw})}$ time series from these N grid cells with the temperature at the target site. The optimal set of cores for each N is then determined from the maximum correlation value across all trials: For $N = 1$, we can directly pick the optimal location from the maximum correlation value within the circle without random sampling; for $N > 1$, we set the maximum number n of picking trials to 10^5 to ensure stable results.

2.3.3 Optimal sampling structure

To learn about the typical spatial scales associated with the processes contributing to the overall temperature–isotope relationship we use a more general approach that reduces local effects in the climate model data. We choose a given target site and define consecutive rings around this site with a $250\,\mathrm{km}$ radial width until a maximum distance of $2000\,\mathrm{km}$ is achieved (Fig. 1). Then, we identify all the grid cells that fall into each of these rings and randomly sample N grid cells from out of these rings. This is implemented in a two-step process: (1) we determine all possible combinations of selecting N rings with replacement,
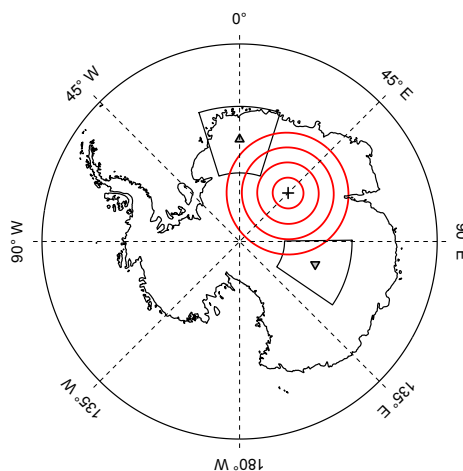
Figure 1. Conceptual sketch of the general approach. Around a given Antarctic target site (black cross), we define consecutive rings (red lines) of 250 km radial width and analyse all model grid cells that fall within each of the rings. Also shown are our main study regions (black polygons) around the EDML (upward pointing triangle) and Vostok (downward pointing triangle) ice-core sites.

115 and then (2) for each ring combination we identify the possibilities of combining grid cells by selecting an individual grid cell from each ring. For each of these grid-cell combinations, we average the time series for a studied model variable (T_{2m}, $T_{2m}^{(pw)}$, $\delta^{18}O^{(pw)}$) and compute the degree of correlation with the target site temperature. Finally, we report the mean correlation for every ring combination by averaging across all correlations of the analysed grid-cell combinations. This provides insight into the average spatial structure of the correlation with the target site temperature for sampling N locations from the model field

120 depending on the distances between the locations. We denote this quantity as the *sampling correlation structure*. Note that in the one-dimensional case ($N = 1$), the sampling correlation structure is identical to what is often called the spatial correlation structure, i.e., the average correlation as a function of distance.

In the second step from the above two-step process, it is computationally feasible to identify all possible grid-cell combinations until $N = 2$. For $N \geq 3$ we resort to Monte Carlo sampling instead, for which we estimated the required number of

125 Monte Carlo iterations from comparing the Monte Carlo sampling solution for $N = 2$ with its exact solution, yielding sufficient convergence for 10^4 iterations. Based on this, we choose 10^5 iterations for sampling $N \geq 3$ locations, since this larger number of locations involves a larger number of possible ring combinations and thus many more possible grid-cell combinations.

2.3.4 Study regions

We focus our analyses predominantly on two subregions of the East Antarctic Plateau, the Dronning Maud Land (DML) region

130 and the Vostok region, both of which include existing deep ice-core drilling sites as well as large arrays of shallower ice and firn cores.

For the DML region, we choose all model grid cells ($N_{\mathrm{grid}} = 26$) within a range of $\pm 17.5°$ longitude and $\pm 5°$ latitude around the European Project for Ice Coring in Antarctica (EPICA) DML site (EDML; $-75°$ S, $0°$ E; Fig. 1). This region encompasses the site of the deep EDML ice core (EPICA community members, 2006; Alfred-Wegener-Institut Helmholtz-Zentrum für Polar-

135 und Meeresforschung, 2016) and > 50 firn and shallow ice cores (Altnau et al., 2015). For the Vostok region, we choose an identical latitudinal and longitudinal coverage ($N_{\mathrm{grid}} = 30$) with respect to the Vostok station ($-78.47°$ S, $106.83°$ E; Fig. 1), encompassing the sites of the deep Vostok and Dome C ice cores and of several shallower cores (Stenni et al., 2017), and the new deep drilling site ("Little Dome C") where an ice core extending back more than one million years is envisaged (Passalacqua et al., 2018).

140 ## 3 Results

3.1 Spatial scale of the temperature anomalies and the local temperature–isotope relationship

First, we asses the extent to which a local ice-core record, i.e., the annual isotope time series of a single grid cell in the model simulation, is representative of the local and regional scale variability of the near-surface atmospheric temperature.

The temperature field over Antarctica in the climate model exhibits large scale coherent variations (Fig. 2) with a clear two-

145 part structure, which is roughly divided by the Transantarctic Mountain range: For most parts of the East Antarctic Plateau, the temperature field shows typical decorrelation lengths between ~ 1500 and $2500\,\mathrm{km}$, while the decorrelation lengths are significantly lower with values $\lesssim 1000\,\mathrm{km}$ for larger parts of the West Antarctic Ice Sheet and for the Antarctic Peninsula. Still, for perfect ice cores, i.e., assuming an ideal temperature proxy record that is only governed by local temperature variations, a single ice core would capture the temperature variability in both East and West Antarctic regions across hundreds of kilometres.

150 However, as simulated by the isotope-enabled climate model, actual single Antarctic ice-core isotope records only explain a low portion of the variations in the local and regional temperature fields: Correlating the annual precipitation-weighted field of modelled $\delta^{18}\mathrm{O}^{(\mathrm{pw})}$, the model variable which most closely mimics a real ice-core record, locally with the annual $T_{2\mathrm{m}}$ time series results in generally low correlations (mean of 0.36), which across all analysed grid cells range from < 0.1 up to ~ 0.53 with $\sim 70\,\%$ of the correlations ≤ 0.4 (Fig. 3a). The correlations are improved when the $T_{2\mathrm{m}}^{(\mathrm{pw})}$ time series is used instead of the

155 $T_{2\mathrm{m}}$ time series with a mean local correlation of 0.51 (range ~ 0 to 0.77; Fig. 3b). This shows that precipitation intermittency is a major limiting factor for the temperature–isotope correlation. In the following sections, we assess the extent to which the correlation with temperature can be increased and how this relates to the spatial scales studied.

3.2 Choosing optimal ice-core sites for temperature reconstructions

The above analysis shows that isotope records from single ice cores likely only capture a small portion of the local interannual

160 temperature variability. This suggests that additional processes, such as precipitation intermittency, influence the isotopic signal and decrease the degree of correlation with the local temperature record. Interpreting these additional processes as noise raises the question of whether the correlation with temperature can be improved upon by averaging isotope records across space. To
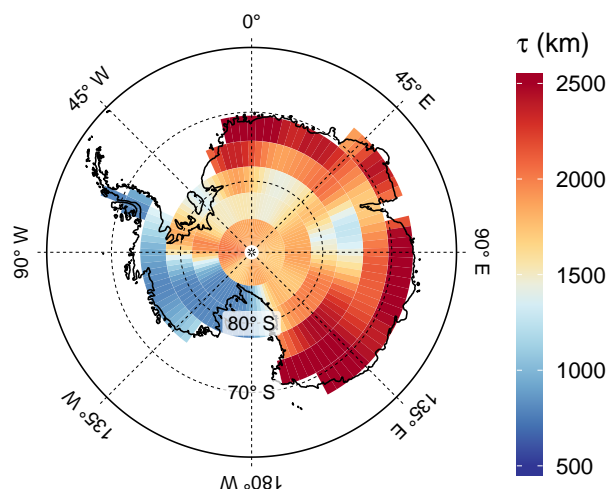
Figure 2. Temperature decorrelation lengths across Antarctica. The temperature decorrelation lengths (τ, in km) for each Antarctic model grid cell were estimated by fitting an exponential model to the correlation–distance relationship (cf. Eq. B4) obtained from correlating the local annual near-surface T_{2m} time series with the respective temperature time series from all other grid cells. Note that only the continental grid cells were used for the fit. Although the decorrelation lengths show a strong partition between East and West Antarctica, they are larger than 1000 km at most locations.

address this question, we assume an ideal world in which the climate model data are a perfect surrogate for the true climate and proxy variations at each site, and set up the simple experiment of randomly picking and averaging $\delta^{18}O^{(pw)}$ grid cells to
165   determine what spatial array of N ice cores optimises the temperature correlation with a target site.

     For our specific model simulation and specifying the EDML drilling site as the target site, we obtain the interesting result that the optimal location for a single ice core is not the local grid cell as one might expect, but a site ~ 1100 km away from the target towards the southeast (Fig. 4a). Choosing this more distant site increases the correlation with the target temperature from an r value of 0.26 for the local EDML site to a value of 0.44. Furthermore, by analysing the maximum correlations with
170   the EDML target temperature for an average of three or five cores (Fig. 4b–c) we find optimal locations that in both cases are scattered at significant distances around the target and which yield an even further increase in correlation ($r = 0.49$ in both cases). We obtain comparable results when the Vostok drilling site is specified as the target (Fig. 4d–f). The optimal single core would be at a location ~ 420 km north of Vostok ($r = 0.45$, compared to the local correlation of $r = 0.34$), and the optimal locations for averaging three or five cores all lie again scattered around the target without including it, and, as for EDML, result
175   in a significant increase in correlation for $N = 3$ ($r = 0.57$) but in no further increase for $N = 5$ ($r = 0.56$).
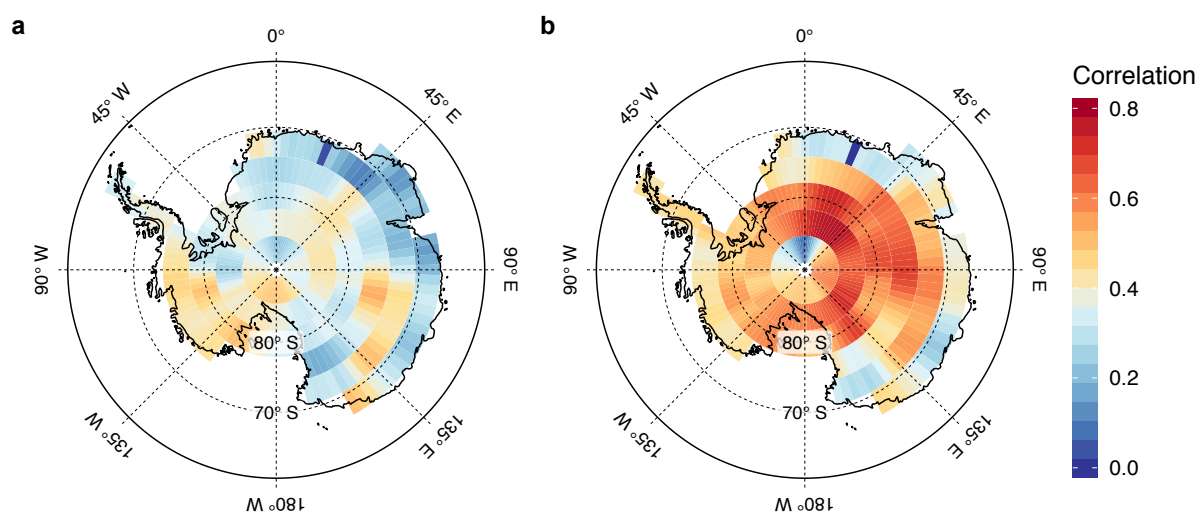
Figure 3. The local temperature–isotope relationship across Antarctica. Shown are the local correlations for each model grid cell between the annual time series of precipitation-weighted oxygen isotope composition and of **(a)** near-surface temperature and **(b)** precipitation-weighted near-surface temperature. The difference between the maps clearly demonstrates that precipitation intermittency is a major limiting factor for the temperature–isotope relationship.

We generalise these findings by considering each Antarctic model grid cell as a target site and determining in each case the ice core location that results in an optimal correlation with the target site. Similarly to the above case studies, the majority ($\sim 67\,\%$) of optimal locations for a single ice core are situated at distances between 400 and $1000\,\mathrm{km}$ from the respective target sites, while only about $20\,\%$ lie within $400\,\mathrm{km}$ from the targets. We note that this distribution might be affected by the number of available sampling points (i.e., model grid cells) per distance bin which increase with increasing distance from the target site.

3.3 Optimal ice-core sampling structures

The approach for choosing optimal ice-core locations yields straightforward and instructive results. However, it might be doubtful as to whether these results can be directly applied to the real world, since they might depend on the specific simulated climate state or result from statistical overfitting. Thus, as a next step, we adapt our approach to learn more about the general spatial arrangement of the optimal ice-core locations which yield the maximum correlation with temperature. To address this issue, we compute the mean of correlation results obtained between a target site temperature and individual grid cells in order to reduce local variability in the model data. We perform this averaging step across several combinations of $250\,\mathrm{km}$ wide concentric rings with a target site at the centre ("sampling correlation structure"; Fig. 1 and Sect. 2.3.3) to derive results which
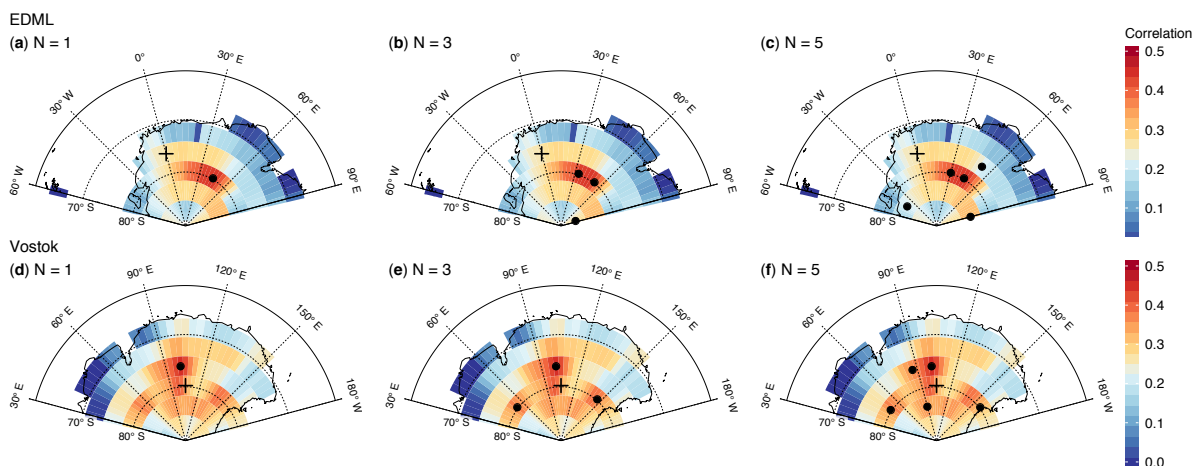
Figure 4. Choosing ice-core locations that optimally reconstruct interannual temperatures at the EDML and Vostok drilling sites. The maps show the correlation coefficient in the climate model data between the annual temperature time series at the target sites (black crosses) EDML (**a–c**) and Vostok (**d–f**) with the time series fields of precipitation-weighted oxygen isotope composition. Filled black circles denote grid cells that maximise the correlation between the target site temperature and either a single grid cell ($N = 1$; **a, d**) or for an average across $N = 3$ (**b, e**) or $N = 5$ (**c, f**) grid cells. Interestingly, non-local ice-core locations systematically show the strongest relationship with the target site temperature.

190   are only a function of radial distance. Additionally, if applicable, we average the obtained results across the target sites within our defined DML and Vostok regions (Sect. 2.3.4) to get regional estimates. Finally, we analyse each of the model variables to highlight the differences between the individual fields.

      The sampling correlation structure from this approach is, when we sample only a single location ($N = 1$), conceptually equivalent to the average correlation with distance, and it therefore simply gives the spatial decorrelation in the case of sampling

195   from the $T_{2\mathrm{m}}$ field itself. Indeed, the sampling correlation structures for $T_{2\mathrm{m}}$ in the DML and Vostok region (Fig. 5) can be described by an exponential decay with a length scale of $\sim 1900\,\mathrm{km}$ in both cases, consistent with the estimated spatial decorrelation lengths on the local scale (Fig. 2). We note that these results show that the maximum average correlation with the target site temperature is obtained from sampling the innermost ring only, consistent with the general expectation.

      When we compare these results to the sampling correlation structure for the $\delta^{18}\mathrm{O}$ field, we find in the DML region a much

200   lower average correlation with the target site temperature as a function of distance (Fig. 5a). The average local ($< 250\,\mathrm{km}$) correlation is ~ 0.4, but decreases only slightly within the first $\sim 1000\,\mathrm{km}$, followed by a little steeper decrease and near constant levels of $r \lesssim 0.2$ for distances $\gtrsim 1700\,\mathrm{km}$. For the Vostok region (Fig. 5b), the sampling correlation structure for $\delta^{18}\mathrm{O}$ exhibits a nearly linear decrease from an initial value of $r \gtrsim 0.5$ to $r \sim 0.1$ in the final ring ($> 2000\,\mathrm{km}$). When we analyse the $\delta^{18}\mathrm{O}^{(\mathrm{pw})}$ fields we find that precipitation weighting overall induces even lower correlation values in both regions, but that it

205   does not have a large effect on the sampling correlation structure itself.
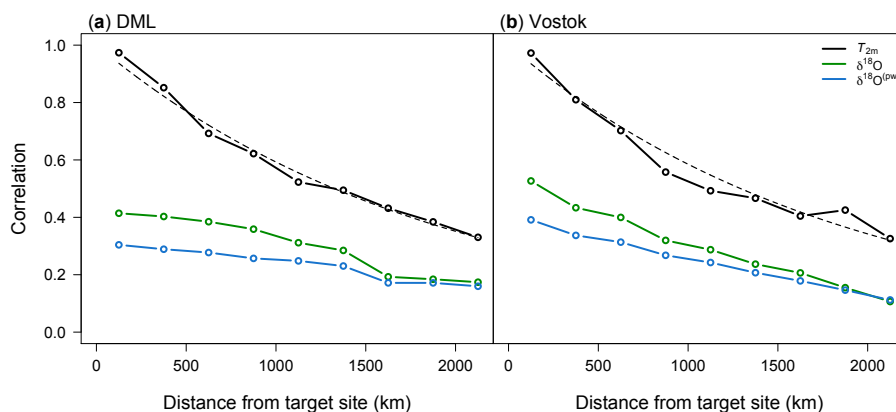
Figure 5. Sampling correlation structures with temperature for the DML and Vostok regions in the case of sampling single locations. Shown is the average correlation as a function of distance between the interannual near-surface temperature ($T_{2\mathrm{m}}$) at a target site and the spatial fields of $T_{2\mathrm{m}}$ (black), oxygen isotope composition ($\delta^{18}\mathrm{O}$, green) and precipitation-weighted oxygen isotope composition ($\delta^{18}\mathrm{O}^{(\mathrm{pw})}$, blue). Averaging was performed in two steps: first, correlations were averaged across grid cells falling within $250\,\mathrm{km}$ wide consecutive rings around a given target site, and secondly, the results were averaged across all respective target sites in the DML **(a)** and Vostok **(b)** region (see Methods). The black dashed lines indicate an exponential fit to the $T_{2\mathrm{m}}$ data.
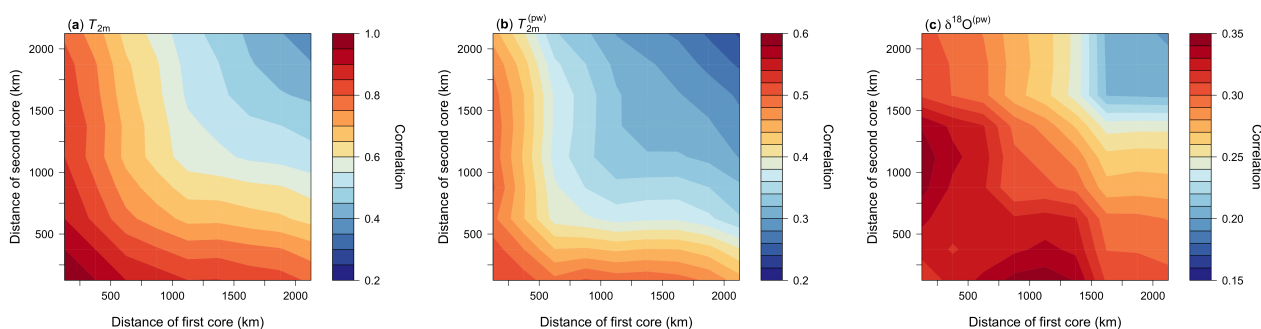
Figure 6. Sampling correlation structure with temperature in the two-dimensional case of sampling two locations in the DML region. Shown is the mean correlation of all possible single correlations for the average of two grid cells of **(a)** $T_{2\mathrm{m}}$, **(b)** $T_{2\mathrm{m}}^{(\mathrm{pw})}$ and **(c)** $\delta^{18}\mathrm{O}^{(\mathrm{pw})}$ time series sampled from the same ring or from two different rings, averaged over all target sites in the given region. The axes display the distance from the target site, where the x (y) axis represents the first (second) sampled ring and the tick marks indicate the midpoint radii of the rings. Note the marked difference in the locations of the correlation maxima between $T_{2\mathrm{m}}$ and $\delta^{18}\mathrm{O}^{(\mathrm{pw})}$.

Extending this analysis to the two-dimensional case of sampling and averaging $N = 2$ locations offers the possibility of investigating the average correlation not only as a function of distance from the target site but also as a function of distance between the two sampled locations (Fig. 6). We find that the difference in the sampling correlation structure between the fields of $T_{2\mathrm{m}}$ and $\delta^{18}\mathrm{O}^{(\mathrm{pw})}$ is even more pronounced for $N = 2$ than for $N = 1$. As one would expect, the maximum average correlation for $T_{2\mathrm{m}}$ is still found when both sampling locations are from the innermost ring, as shown for the DML region

210
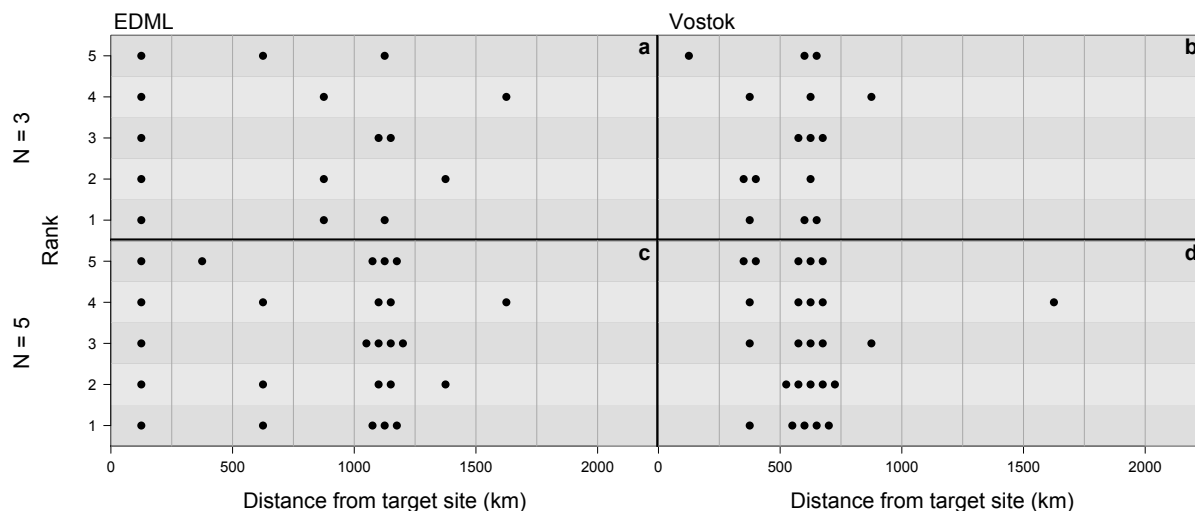
Figure 7. The optimal arrangement for averaging three or five $\delta^{18}O^{(pw)}$ ice cores to reconstruct the target site temperature at the EDML **(a, c)** and Vostok **(b, d)** drilling sites. Displayed are subsets of the sampling correlation structures for $N = 3$ and 5, showing along the vertical axis the optimal five of all possible combinations of rings, i.e., those which exhibit the highest mean correlation across 10^5 random trials of averaging $N = 3$ **(a, b)** or $N = 5$ **(c, d)** grid cells from these rings. The ring bin borders are marked by thin vertical lines with their distances from the target site given on the horizontal axis; the selected optimal ring combinations are marked as black dots. Systematically, arrangements with several ice cores sampled at 500 to 1000 km distances are found to be optimal.

(Fig. 6a). However, for $\delta^{18}O^{(pw)}$ the optimal arrangement of two locations to obtain the maximum average correlation is to sample one location from the innermost ring and the second location from the fifth ring, i.e., between ~ 1000 and 1250 km from the target site (Fig. 6c). Part of this structure is related to the effect of precipitation intermittency, which can be seen from the sampling correlation structure of the $T_{2m}^{(pw)}$ field (Fig. 6b). Here, in contrast to T_{2m}, the correlation is about as high when

215 we combine the innermost ring and one ring further away, as when we sample both locations from the innermost ring.

Analysing the Vostok study region leads to comparable results (Appendix A: Fig. A1), with a similar difference in sampling correlation structure between T_{2m} and $T_{2m}^{(pw)}$ as for the DML region, and a similar structure of $T_{2m}^{(pw)}$ and $\delta^{18}O^{(pw)}$ for distances $\lesssim 1000$ km. However, the results for the $\delta^{18}O^{(pw)}$ field (Fig. A1c) do not display such a pronounced maximum correlation when one location is sampled from the innermost ring and the second one from a ring further away as is observed for the DML

220 region. This suggests the regional differences in the spatial correlation structure of the $\delta^{18}O$ field (Fig. 5) to have an influence here.

The general feature of the optimal $\delta^{18}O^{(pw)}$ sampling arrangement is robust throughout Antarctica, despite the above regional differences. When we analyse all available Antarctic target sites, setting the first location to the innermost ring and looking for an optimal ring of the second location, in which the average correlation with the target site temperature is maximal,

225 we find that in $\sim 77\%$ of all cases the optimal configuration for the second location is at least the second ring (> 250 km), and in $\sim 61\%$ of the cases it is within the second to fourth ring (250–1000 km).

Furthermore, we obtain similar results also when averaging $N = 3$ or 5 locations of the $\delta^{18}\mathrm{O}^{(\mathrm{pw})}$ field to reconstruct the target site temperature (Fig. 7). When EDML is set as the target site, the optimal sampling configuration is such that one location lies in the innermost ring while the others are distributed at distances between ~ 500 and $1500\,\mathrm{km}$ from the target.

230   For reconstructing the Vostok target site temperature, the optimal locations are mostly distributed across the second to third (250–750 km) ring.

In summary, averaging the $\delta^{18}\mathrm{O}^{(\mathrm{pw})}$ time series across several locations clearly increases the average correlation with the target site temperature, if this averaging follows an optimal combination of rings, as compared to sampling all locations only locally (Fig. 8a). The increase in correlation becomes larger by averaging more locations: while the local correlation stays

235   constant at 0.27 (EDML) and 0.34 (Vostok), the optimal correlation rises for $N = 2$ to 0.32 and 0.40, respectively, and for $N = 10$ to 0.39 and 0.49. This is equivalent to nearly a doubling in the explained variance.

We note that these results are the mean value from averaging across many possible combinations of individual locations. In reality, any new drilling campaign or reanalysis of existing ice cores only represents one single combination of locations. Therefore, we assess the risk of an "adverse optimal sampling", i.e., the probability of choosing by chance a specific sampling

240   realisation from the optimal ring combination which yields a lower correlation than the correlation for sampling locally. For this purpose, we compare the distribution of individual correlations from sampling the optimal ring combination with the value obtained from sampling only the local sites which lie in the innermost ring. Overall we find the risk of adverse optimal sampling to be low, since more than $92\,\%$ of all individual correlation values in the example of $N = 3$ are actually larger than the respective local correlation (Fig. 8b).

245   ## 4   Discussion

Oxygen isotope records derived from ice cores are commonly interpreted to reflect local temperature changes at the ice-core drilling site. Here, in a systematic study of analysing the interannual correlation between precipitation-weighted oxygen isotope composition and near-surface atmospheric temperature in a climate model, we showed that while there is local isotope–temperature correlation (Fig. 3a), this correlation can be increased considerably by averaging isotope records across space

250   (Fig. 8a) following a distinct spatial pattern which combines the local target site with locations located between a few hundred kilometres to up to $\sim 1000\,\mathrm{km}$ from the target site (Figs. 6c, 7 and A1c). In the next section, we develop a qualitative understanding of these results from a conceptual model that predicts the sampling correlation structure from the processes that shape the isotopic composition time series, before discussing the relevance of our results to actual ice-cores studies.

4.1   Conceptual model of the optimal sampling structure

255   For a conceptual model of the sampling correlation structure, we focus on three processes that influence the oxygen isotope records in ice cores: (i) temperature variations, (ii) precipitation intermittency, and (iii) the temperature–isotope relationship. We statistically model the associated fields of $T_{2\mathrm{m}}$, $T_{2\mathrm{m}}^{(\mathrm{pw})}$ and $\delta^{18}\mathrm{O}^{(\mathrm{pw})}$ separately in order to understand the influence of each process (see Appendix B for details), and we assess, for comparable results, the predicted average sampling correlation
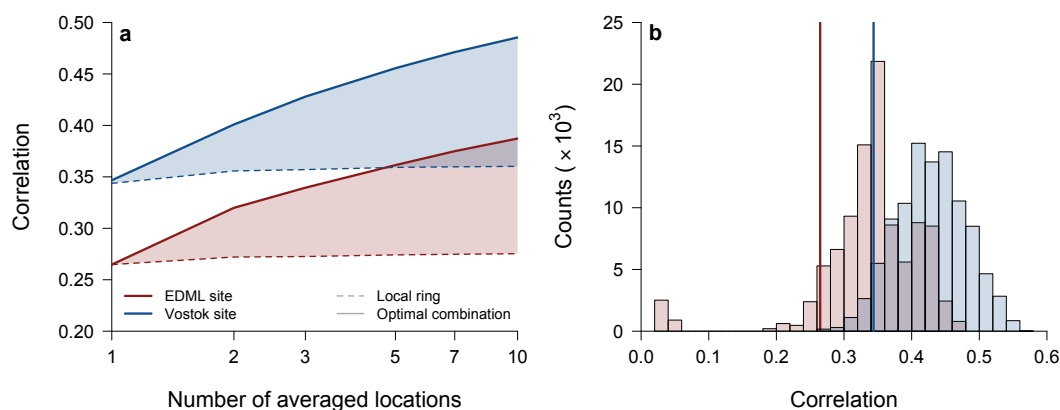
Figure 8. Gain in correlation and risk of adverse sampling. **(a)** The average correlation with the target temperature at the EDML (red) and Vostok (blue) sites depending on the number of locations, N, used for averaging the $\delta^{18}O^{(pw)}$ time series. Sampling is performed either locally from the innermost ring only (dashed lines), or from all possible individual combinations of locations for the respective optimal ring combination determined for each N (solid lines). Compared to the local samples which show virtually no increase with the number of sampled locations, the correlation increases markedly with N when sampling from the optimal rings, as highlighted by the shaded area. **(b)** Histogram of individual correlations for sampling from the optimal ring combination when averaging $N = 3$ locations compared to the correlation (vertical lines) for sampling from the innermost ring only, displayed for the EDML (red) and Vostok (blue) target sites. For more than $90\,\%$ of the optimal ring combination samples, the correlation is higher than the local value.

structure with the target site temperature in the two-dimensional case of averaging two locations in the same manner that we

260   analysed the climate model data.

To model the atmospheric temperature field, we assume an isotropic exponential decay of the spatial correlation with a constant decorrelation length (Appendix B2). Such an exponential temperature decorrelation is a commonly observed feature (Jones et al., 1997) and also confirmed by our climate model data (Figs. 2 and 5). Given this relationship, we find a good agreement for the two-dimensional sampling correlation structure between the conceptual model and the climate model data,

265   both regarding absolute correlation values as well as the spatial pattern (Fig. B1a). We emphasise that the maximum correlation with the target site temperature naturally occurs, in case of an isotropic correlation decay, when the averaged two (or N) locations are close to the target site, as any location which is further away will result in a temperature signal that is less similar between the locations.

To elucidate the role of precipitation intermittency, we follow the simplest assumption which is that this process can be

270   described by partly aliasing the original temperature signal into temporal white noise (Laepple et al., 2018; Casado et al., 2020). We further assume that this noise is not independent between sites but that it follows the spatial scale of precipitation events, which we describe as an exponential decorrelation in space with a second length scale (Appendix B3). This intermittency length scale is related to the atmospheric processes that deliver precipitation, e.g., synoptic systems, and is hence assumed to be smaller than the length scale of the temperature anomalies. The introduction of this second length scale into our conceptual model

275 generally explains the optimal sampling structure we obtained from the climate model data. Qualitatively, close-by locations exhibit a strong correlation in temperature but also in the noise from precipitation intermittency; therefore, this noise cannot be reduced by averaging the locations, yielding an overall low signal-to-noise ratio. However, with increasing distance between the locations, the intermittency noise decorrelates faster than the temperature field due to the different decorrelation scales, resulting in an optimal distance of maximum signal-to-noise ratio. This is also reflected in our conceptual model (Fig. B1b, e).

280 When fixing one location to the target site and varying the distance from the target site of the second location, the correlation with the target site temperature first increases with increasing distance of the second location and then maximises at an optimal distance, before it decays with a further increase in distance. In the climate model data, we observed a similar feature for the precipitation-weighted temperature (Figs. 6 and A1), though it was not as clear as in the conceptual model. This mismatch could be related to the assumed isotropy in the conceptual model and the according azimuthal averaging done in the climate

285 model data analysis, which potentially smears the intermittency effect in the climate model data due to slight differences in the decorrelation lengths between the different horizontal directions.

In order to incorporate the $\delta^{18}O^{(\mathrm{pw})}$ field into the conceptual model, we need to account for the spatial temperature–isotope relationship. To accomplish this, we parameterise the spatial dependence of the correlation between temperature and the oxygen isotope composition with a simple isotropic linear model based on the climate model data results (Fig. 5 and Appendix B4).

290 In addition, we assume that the same effect of precipitation intermittency that we adopted for the temperature field is also applicable to the oxygen isotope field. With these simple assumptions, we obtain a good qualitative agreement for the DML region between the conceptual model and the climate model data results (cf. Figs. B1c and 6c). In addition, when we change the parameterised isotope–temperature relationship such that it more closely resembles the Vostok region data (Fig. 5b), the sampling correlation structure in the conceptual model (Fig. B1f) is more similar to the observed correlation structure (Fig. A1c).

295 However, in general the conceptual model fails for $\delta^{18}O^{(\mathrm{pw})}$ to reproduce the actual range in correlations as it produces much lower values than expected.

In summary, our conceptual model provides a quantitative understanding of the spatial correlation of the temperature in the climate model data, and, at least, a qualitative understanding of the processes that affect the correlation between temperature and the $\delta^{18}O^{(\mathrm{pw})}$ field, i.e., precipitation intermittency and the spatial temperature–isotope relationship. The deficiencies in

300 the conceptual model may be attributed to its simplicity. For the governing processes, we assumed spatially constant and isotropic length scales, neglecting local and direction-related differences in, e.g., temperature decorrelation lengths (cf. Fig. 2) or the spatial extent of the coherence of precipitation intermittency. Instead of being constant, the latter may differ depending on the type of precipitation, e.g., synoptic versus clear-sky precipitation, and may exhibit directional dependencies related to topography. Furthermore, we assumed constant variance for all time series, thereby ignoring potential weighting effects on the

305 correlations for the spatial average of several locations due to different variabilities between them.

4.2 Relevance for ice-core studies

Our results which we obtained from analysing the climate model data and substantiated with our conceptual model provide guidance on where to drill $N = 1, 2, 3$ or more ice cores, or from which locations to analyse them, in order to optimally reconstruct the atmospheric temperature signal for a certain target site or region.

310   The first possibility is to follow the recommendations obtained from directly choosing the specific locations which maximise the correlation with the target site temperature (Fig. 4). However, it is unclear whether these results can be one-to-one transferred to the real world, since they might depend on dynamical processes in the atmosphere which could differ between climate states or depend on initial conditions. One indication for this is that we obtain different optimal single core locations for more than half of all investigated Antarctic target sites, when we analyse only the first or the second half of the respective

315   climate model time series as compared to the full 1200 years.

     Here we argue that the optimal spatial sampling configuration is on average governed by the interplay of the different underlying correlation length scales, which we expect to vary less in between different climate periods or states. This is substantiated by the fact that the sampling correlation structures for two cores (Figs. 6 and A1), obtained from averaging the correlations from individual sampling locations across concentric rings around the target site, are much more robust against

320   analysing only the first or the second half of the model time series, different to the results from directly choosing optimal locations.

     Using the sampling correlation structures we arrive at the following recommendations for optimal ice core sampling configurations. If it is only possible to drill or analyse a single ice core, our results show that it is always best to sample locally, i.e., to place this core near the target site of interest. This is also common practice, given the usual interpretation of ice-core isotope

325   records as a proxy for local temperatures. However, due to the effect of precipitation intermittency, in the case of drilling two ice cores it is no longer optimal to collect both cores near the target site, but instead to drill one core at the target site and one at least $500\,\mathrm{km}$ away. Where three or more ice cores will be drilled or analysed, we expect the optimal spatial configuration to be more dependent on the study region. However, our results indicate that in general it is still likely better to place one core near the target site and distribute the others across several hundreds of kilometres.

330   These inferences are based on data from a single climate model simulation together with a simple statistical conceptual model, which should be tested against observations. We thus need to create an isotope record that is in first order only governed by temperature variations and precipitation intermittency, and remove the impact of local stratigraphic noise from the actual measured records (assuming that any further processes in the pre-depositional to depositional phase contribute negligibly to the local isotopic variations). To accomplish this one possible strategy would be to use trench sampling campaigns (see Münch

335   et al., 2016, 2017 for the EDML site). Then, one test of our optimal sampling configurations could be to combine one trench record, e.g., one from EDML, with another trench sampled at the optimal distance based on our results for $N = 2$, and correlate the average of these two trench records with the instrumental temperature data set available for EDML. Based on the results in this study we would expect a higher degree of correlation in this case compared to using only one local trench record from

EDML. We acknowledge that such an approach would be challenging due to the small amount of available instrumental data

340 (~ 20 years for EDML) and by the inevitable dating uncertainties between the two trench records.

5 Conclusions

In this study we assessed the spatial sampling configuration of ice cores to optimally reconstruct the annual near-surface temperature at a specific target site. This problem was motivated by the expectation that the major processes influencing the isotopic records of ice cores operate on different spatial scales.

345 Indeed, by analysing the temperature and isotope data of an isotope-enabled atmosphere–ocean climate model simulating the climatic history over the last millennium in Antarctica, we showed that while in the optimal setup a single ice core should be placed close to the target site of interest, a second core should be located far (> 500 km) from the first core. While this may seem surprising at first glance, it can be straightforwardly explained by the interplay of two different correlation lengths in space: one for the temperature anomalies and one parameterising the spatial coherence of the effect of precipitation intermittency, as

350 demonstrated by a simple conceptual model. Despite the fact that these results were specifically obtained for two regions of the East Antarctic Plateau, we expect similar results to hold for other parts of Antarctica, and potentially also for other large-scale ice-coring regions such as Greenland.

Our study therefore explicitly improves the planning of drilling or analysis campaigns for spatial networks of ice-core isotope records. In addition, it provides a strategy to analyse an optimal configuration of sampling locations for any proxy which is

355 influenced by two or more processes that exhibit different spatial correlation scales. This likely applies to various marine as well as terrestrial proxy types, and our strategy thus might offer a step forward in the best use of sampling and measurement capacity for quantitative climate reconstructions.

Code and data availability. The climate model data used in this study is freely available from the Zenodo database under https://doi.org/10. 5281/zenodo.4001565 (Münch and Werner, 2020). Software to run the analyses and produce the figures is available as R code hosted in the

360 public git repository at https://github.com/EarthSystemDiagnostics/optimalcores. A snapshot of the software code will be archived on the Zenodo database once the paper is accepted.

Appendix A: Two-dimensional sampling correlation structure for the Vostok region

In order to reduce the number of figures in the main text, we provide the results of the average two-dimensional sampling correlation structures ($N = 2$) for the Vostok study region here in Fig. A1.
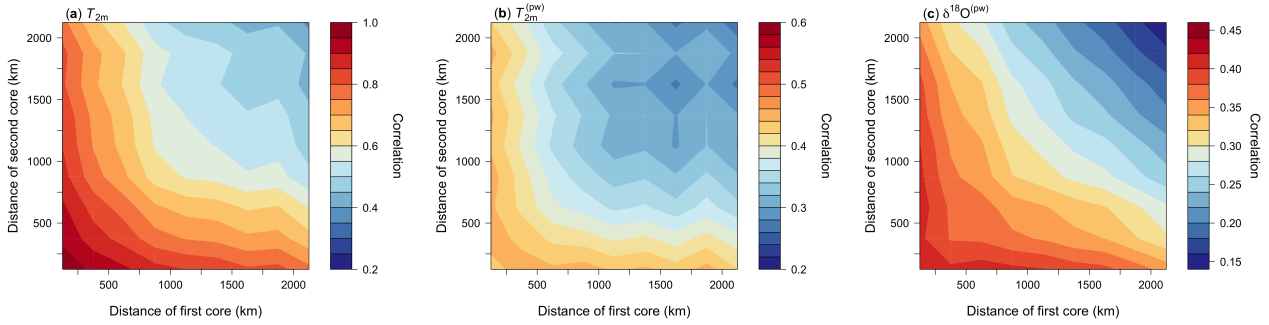
Figure A1. Same as Fig. 6 but for the Vostok region. Note that for $\delta^{18}\text{O}^{(\text{pw})}$ the – albeit marginal – correlation maximum is achieved by combining the innermost ring with the ring between 500–$750\,\text{km}$.

Appendix B: Conceptual model of sampling correlation structures

B1   General model

We set up a conceptual model for the correlation between a target temperature time series and a spatial average based on a set of locations sampled from a climatic field (sampling correlation structure). Our model assumes simple isotropic and exponential decorrelation structures for the involved climatic fields and is based on previous work which suggests that precipitation intermittency can be described by partly aliasing the original temperature signal into white noise (Laepple et al., 2018).

In the model, we consider a temperature time series T_0 at some target site $\mathbf{r}_0$ and a field x of a given climate variable. From this field, we select N time series x_i at the locations $\mathbf{r}_i$, $i = 1, \ldots, N$, and denote the spatial average of these time series by $\overline{x} = \frac{1}{N} \sum_{i=1}^{N} x_i$. The distances of the N locations from the target site and the distances between the locations are given by $r_i = |\mathbf{r}_i - \mathbf{r}_0|$ and by $d_{ij} = |\mathbf{r}_i - \mathbf{r}_j|$, respectively. The correlation between T_0 and $\overline{x}$ follows from

$$\text{cor}(T_0, \overline{x}) = \frac{\text{cov}(T_0, \overline{x})}{\sqrt{\text{var}(T_0)\text{var}(\overline{x})}}, \tag{B1}$$

and it is governed by the covariance between the temperature at the target site and the climate field at the sampling locations $\mathbf{r}_i$,

$$\text{cov}(T_0, \overline{x}) = \frac{1}{N} \sum_{i}^{N} \text{cov}(T_0, x_i), \tag{B2}$$

and by the covariance between the sampling locations through the variance of their spatial average,

$$\text{var}(\overline{x}) = \frac{1}{N^2} \left(\sum_{i}^{N} \text{var}(x_i) + 2 \sum_{i}^{N-1} \sum_{j}^{N} \text{cov}(x_i, x_j) \right). \tag{B3}$$

In our model, these quantities depend on the distance between sites and on the correlation structure of the respective field x, as we show in the following.

B2 Temperature

For the near-surface temperature field, $x \equiv T$, we assume a spatially constant variance, $\mathrm{var}(T_0) = \mathrm{var}(T_i) \equiv \sigma_T^2$, and an isotropic decorrelation following an exponential decay with a decorrelation length τ; i.e., the covariance between sites is

$$\mathrm{cov}(T_0, T_i) = \sigma_T^2 \exp\left(-\frac{r_i}{\tau}\right), \tag{B4}$$

$$\mathrm{cov}(T_i, T_j) = \sigma_T^2 \exp\left(-\frac{d_{ij}}{\tau}\right). \tag{B5}$$

The correlation between the target site temperature and the spatial average of N temperature time series is then obtained from

$$\mathrm{cor}(T_0, \overline{T}) = \frac{\sum_{i=1}^{N} \exp\left(-\frac{r_i}{\tau}\right)}{\sqrt{N + 2\sum_{i=1}^{N-1}\sum_{j=i+1}^{N} \exp\left(-\frac{d_{ij}}{\tau}\right)}}. \tag{B6}$$

B3 Precipitation-weighted temperature

To model the effect of precipitation intermittency, we follow Laepple et al. (2018) and assume that precipitation intermittency redistributes the energy of the temperature time series constantly across frequencies, i.e., creating temporal white noise without changing the total variance. Then, the precipitation-weighted temperature time series at location $\mathbf{r}_i$ arises from T_i as

$$T_i^{(\mathrm{pw})} = (1-\xi)^{1/2} T_i + \xi^{1/2} \sigma_T \varepsilon_i(0,1), \tag{B7}$$

where $\varepsilon_i(0,1)$ are independent and normally distributed random variables with a mean of zero and a standard deviation of 1. The parameter $0 \leq \xi \leq 1$ determines the fraction of the input temperature time series which is aliased into white noise.

The covariance between the target site temperature and a precipitation-weighted temperature time series is then

$$\mathrm{cov}(T_0, T_i^{(\mathrm{pw})}) = (1-\xi)^{1/2} \sigma_T^2 \exp\left(-\frac{r_i}{\tau}\right), \tag{B8}$$

which implies that the spatial correlation structure between T_0 and the precipitation-weighted temperature follows the same exponential decay as in Eq. (B4), only scaled by the factor $(1-\xi)^{1/2}$. The factor ξ can be estimated from the climate model data by analysing the local correlation, i.e., at the same grid cell, between the temperature and the precipitation-weighted temperature.

We further assume that the effect of precipitation intermittency is not independent between sites but is related to the spatial coherence of the precipitation fields, for which we assume an exponential decorrelation structure with a decay length τ_{pw}. Based on these assumptions, the spatial covariance between sites of the white noise terms induced by the effect of precipitation intermittency has the form

$$\mathrm{cov}(\varepsilon_i, \varepsilon_j) = \exp\left(-\frac{d_{ij}}{\tau_{\mathrm{pw}}}\right). \tag{B9}$$

Then, the correlation between the target site temperature and the spatial average of N precipitation-weighted temperature time series is governed by the intermittency factor ξ and by the two spatial length scales τ and τ_{pw},

$$\mathrm{cor}\left(T_0, \overline{T}^{(\mathrm{pw})}\right) = \frac{\sqrt{1-\xi}\sum_{i=1}^{N} \exp\left(-\frac{r_i}{\tau}\right)}{\sqrt{N + 2\sum_{i=1}^{N-1}\sum_{j=i+1}^{N} g(d_{ij}; \tau, \tau_{\mathrm{pw}}, \xi)}}, \tag{B10}$$

with

$$g(d_{ij}; \tau, \tau_{\mathrm{pw}}, \xi) := (1 - \xi) \exp\left(-\frac{d_{ij}}{\tau}\right) + \xi \exp\left(-\frac{d_{ij}}{\tau_{\mathrm{pw}}}\right). \tag{B11}$$

B4 Precipitation-weighted oxygen isotope composition

For the precipitation-weighted oxygen isotope composition field, $x \equiv \delta^{(\mathrm{pw})}$, we assume the same effect of precipitation in-
415 termittency as on the temperature field. Furthermore, an analysis of the climate model data suggests that the oxygen isotope
field largely exhibits an exponential decorrelation structure in space (not shown). Hence, the correlation between the target site
temperature and the spatial average of N $\delta^{(\mathrm{pw})}$ time series is obtained in a similar manner as for $T^{(\mathrm{pw})}$, i.e.,

$$\mathrm{cor}\left(T_0, \overline{\delta}^{(\mathrm{pw})}\right) = \frac{\sqrt{1 - \xi} \sum_{i=1}^{N} \mathrm{cor}\left(T_0, \delta_i\right)}{\sqrt{N + 2 \sum_{i=1}^{N-1} \sum_{j=i+1}^{N} g(d_{ij}; \tau_\delta, \tau_{\mathrm{pw}}, \xi)}}, \tag{B12}$$

where τ_δ is the decorrelation length of the δ field and the only difference to Eq. (B10) is the unknown spatial correlation
420 structure between the temperature at the target site and the oxygen isotope field, $\mathrm{cor}\left(T_0, \delta_i\right)$. Based on our climate model
results (Fig. 5), we parameterise this function with a simple linear decay of the form

$$\mathrm{cor}\left(T_0, \delta_i\right) = \begin{cases} c_0 - \gamma d, & d \le d_0, \\ 0, & d > d_0, \end{cases} \tag{B13}$$

where $\gamma = c_0 / d_0$ and d_0 is some threshold distance above which the correlation is zero.

B5 Model parameter estimation and model results

425 Overall, our model is governed by three decorrelation lengths (τ, τ_δ, τ_{pw}), the intermittency factor ξ, and two parameters
describing the temperature–isotope correlation (c_0, d_0).

We estimate τ from the climate model data for the DML and Vostok regions (Fig. 5) and find for both regions values of
$\tau = 1900\,\mathrm{km}$. In the same way we estimate a value of $\tau_\delta = 1100\,\mathrm{km}$ for both regions. The intermittency factor ξ is derived
from the local correlation between temperature and precipitation-weighted temperature (Eq. B8). We find an average value
430 for the DML region of $\xi_{\mathrm{DML}} = 0.73$, which is close to the average value across all of Antarctica ($\xi_{\mathrm{Ant.}} = 0.71$), while the
intermittency is stronger for the Vostok region ($\xi_{\mathrm{Vostok}} = 0.82$). We parameterise the temperature–isotope correlation in the
DML region with $c_0 = 0.4$ and $d_0 = 6000\,\mathrm{km}$ and in the Vostok region with $c_0 = 0.5$ and $d_0 = 2500\,\mathrm{km}$ (Fig. 5). The only
unconstrained parameter is the decorrelation length of the effect of precipitation intermittency, τ_{pw}, since it is unclear by
which precipitation variable it is mainly governed (total annual amount, seasonal amount, or its distribution). An investigation
435 with reanalysis data yielded scales between ~ 300 to $500\,\mathrm{km}$ for different precipitation variables (Münch and Laepple, 2018),
while our model data exhibits an average decorrelation length of $\sim 600\,\mathrm{km}$ for the annual precipitation amount. Here, for the
conceptual model we choose a value of $500\,\mathrm{km}$.

We can test our assumption for the effect of intermittency based on using the estimated values of τ and ξ to predict the
spatial decorrelation between temperature and precipitation-weighted temperature (Eq. B8). Indeed, this yields a comparably
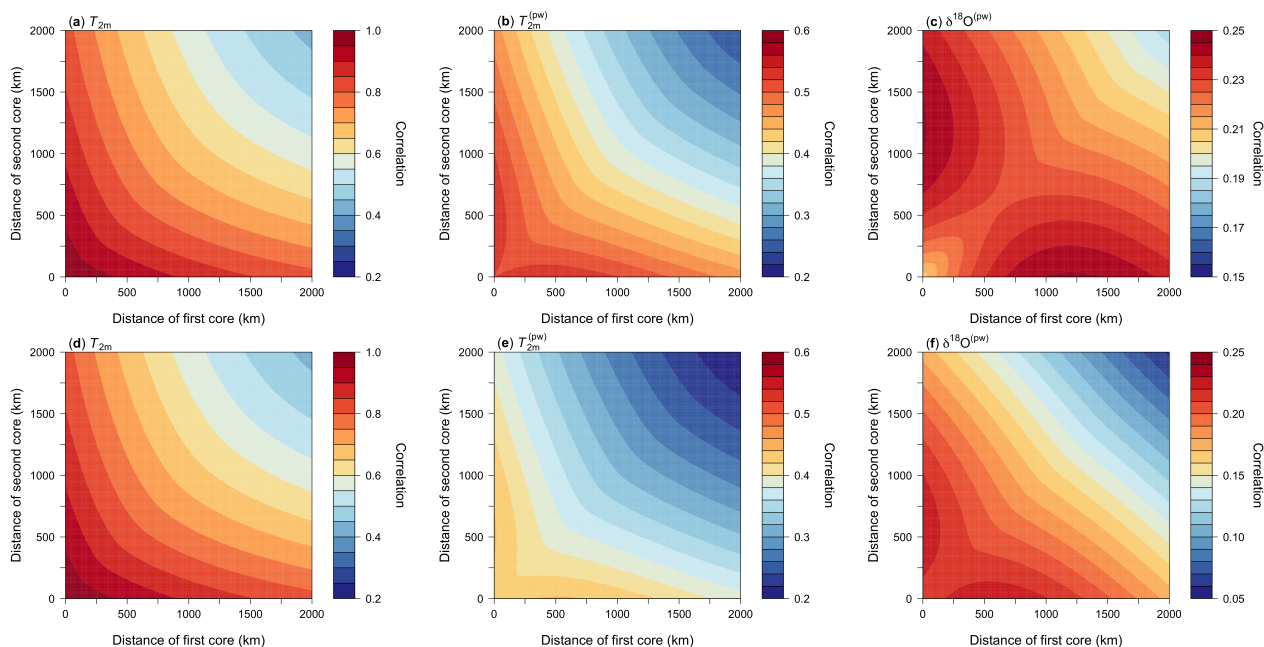
Figure B1. Two-dimensional sampling correlation structures with temperature as predicted from our conceptual model using the model parameters from the DML **(a–c)** and Vostok **(d–f)** regions. Shown is the mean correlation of all possible single correlations for the average of two time series sampled from a pair of concentric rings around the target site for the fields of **(a, d)** T_{2m}, **(b, e)** $T_{2m}^{(pw)}$ and **(c, f)** $\delta^{18}O^{(pw)}$. Note that the plots **(a)** and **(c)** are based on the same parameters and therefore identical.

440 good fit to the data as an independent fit (root mean square deviation of ~ 0.03 between data and fit in both cases), supporting our assumption that intermittency can be parameterised by a partial conversion of the time series into white noise.

Similarly to analysing the climate model data, we now use our conceptual model to predict the two-dimensional ($N = 2$) sampling correlation structures for the different model fields of T_{2m}, $T_{2m}^{(pw)}$ and $\delta^{18}O^{(pw)}$ (Eqs. B6, B10 and B12). Since our model space is continuous, we sample from locations placed *on* concentric rings around the target site. We either sample the

445 two locations from the same ring or from two different rings, using ring radii from 0 to 2000 km in increments of 10 km, and calculate the average correlation for a specific ring combination. To obtain meaningful expectation values, we choose 36 locations distributed uniformly across each ring in steps of $10°$, combine these locations one by one for each ring combination, and average across the correlations for each location pair. With the model parameters from the DML and Vostok regions we obtain the results displayed in Fig. (B1), which are discussed and compared to the estimated results from the climate model

450 data in the main text.

Acknowledgements. We thank Jesper Sjolte (Lund University) for performing the ECHAM5/MPI-OM-wiso past1000 model simulation, and Mathieu Casado, Raphaël Hébert and Torben Kunz (AWI) for their helpful comments on this project. All plots and numerical analyses in this paper were carried out using the open-source software R: A Language and Environment for Statistical Computing.

References

455   Alfred-Wegener-Institut Helmholtz-Zentrum für Polar- und Meeresforschung: Neumayer III and Kohnen Station in Antarctica operated by
the Alfred Wegener Institute, Journal of large-scale research facilities, 2, https://doi.org/10.17815/jlsrf-2-152, 2016.

Altnau, S., Schlosser, E., Isaksson, E., and Divine, D.: Climatic signals from 76 shallow firn cores in Dronning Maud Land, East Antarctica,
The Cryosphere, 9, 925–944, https://doi.org/10.5194/tc-9-925-2015, 2015.

Birks, S. J. and Edwards, T. W. D.: Atmospheric circulation controls on precipitation isotope–climate relations in western Canada, Tellus B,
460   61, 566–576, https://doi.org/10.1111/j.1600-0889.2009.00423.x, 2009.

Casado, M., Münch, T., and Laepple, T.: Climatic information archived in ice cores: impact of intermittency and diffusion on the recorded
isotopic signal in Antarctica, Clim. Past, 16, 1581–1598, https://doi.org/10.5194/cp-16-1581-2020, 2020.

Craig, H. and Gordon, L. I.: Deuterium and oxygen 18 variations in the ocean and the marine atmosphere, in: Stable Isotopes in Oceano-
graphic Studies and Paleotemperatures, edited by Tongiorgi, E., Proceedings Spoleto 1965, pp. 9–130, V. Lishi e F., Pisa, 1965.

465   Dansgaard, W.: Stable isotopes in precipitation, Tellus, 16, 436–468, https://doi.org/10.3402/tellusa.v16i4.8993, 1964.

EPICA community members: One-to-one coupling of glacial climate variability in Greenland and Antarctica, Nature, 444, 195–198,
https://doi.org/10.1038/nature05301, 2006.

Fisher, D. A., Reeh, N., and Clausen, H. B.: Stratigraphic Noise in Time Series Derived from Ice Cores, Ann. Glaciol., 7, 76–83,
https://doi.org/10.1017/S0260305500005942, 1985.

470   Goursaud, S., Masson-Delmotte, V., Favier, V., Orsi, A., and Werner, M.: Water stable isotope spatio-temporal variability in Antarctica
in 1960–2013: observations and simulations from the ECHAM5-wiso atmospheric general circulation model, Clim. Past, 14, 923–946,
https://doi.org/10.5194/cp-14-923-2018, 2018.

Jones, P. D., Osborn, T. J., and Briffa, K. R.: Estimating Sampling Errors in Large-Scale Temperature Averages, J. Clim., 10, 2548–2568,
https://doi.org/10.1175/1520-0442(1997)010<2548:ESEILS>2.0.CO;2, 1997.

475   Joussaume, S., Sadourny, R., and Jouzel, J.: A general circulation model of water isotope cycles in the atmosphere, Nature, 311, 24–29,
https://doi.org/10.1038/311024a0, 1984.

Jouzel, J. and Merlivat, L.: Deuterium and Oxygen 18 in Precipitation: Modeling of the Isotopic Effects During Snow Formation, J. Geophys.
Res., 89, 11 749–11 757, https://doi.org/10.1029/JD089iD07p11749, 1984.

Küttel, M., Steig, E. J., Ding, Q., Monaghan, A. J., and Battisti, D. S.: Seasonal climate information preserved in West Antarctic ice core water
480   isotopes: relationships to temperature, large-scale circulation, and sea ice, Clim. Dyn., 39, 1841–1857, https://doi.org/10.1007/s00382-
012-1460-7, 2012.

Laepple, T., Werner, M., and Lohmann, G.: Synchronicity of Antarctic temperatures and local solar insolation on orbital timescales, Nature,
471, 91–94, https://doi.org/10.1038/nature09825, 2011.

Laepple, T., Hörhold, M., Münch, T., Freitag, J., Wegner, A., and Kipfstuhl, S.: Layering of surface snow and firn at Kohnen Station,
485   Antarctica: Noise or seasonal signal?, J. Geophys. Res. Earth Surf., 121, 1849–1860, https://doi.org/10.1002/2016JF003919, 2016.

Laepple, T., Münch, T., Casado, M., Hoerhold, M., Landais, A., and Kipfstuhl, S.: On the similarity and apparent cycles of isotopic variations
in East Antarctic snow pits, The Cryosphere, 12, 169–187, https://doi.org/10.5194/tc-12-169-2018, 2018.

Lorius, C., Merlivat, L., and Hagemann, R.: Variation in the Mean Deuterium Content of Precipitations in Antarctica, J. Geophys. Res., 74,
7027–7031, https://doi.org/10.1029/JC074i028p07027, 1969.

490 Masson-Delmotte, V., Hou, S., Ekaykin, A., Jouzel, J., Aristarain, A., Bernardo, R. T., Bromwich, D., Cattani, O., Delmotte, M., Falourd, S., Frezzotti, M., Gallée, H., Genoni, L., Isaksson, E., Landais, A., Helsen, M. M., Hoffmann, G., Lopez, J., Morgan, V., Motoyama, H., Noone, D., Oerter, H., Petit, J. R., Royer, A., Uemura, R., Schmidt, G. A., Schlosser, E., Simões, J. C., Steig, E. J., Stenni, B., Stievenard, M., van den Broeke, M. R., van de Wal, R. S. W., van de Berg, W. J., Vimeux, F., and White, J. W. C.: A Review of Antarctic Surface Snow Isotopic Composition: Observations, Atmospheric Circulation, and Isotopic Modeling, J. Climate, 21, 3359–

495 3387, https://doi.org/10.1175/2007JCLI2139.1, 2008.

Münch, T. and Laepple, T.: What climate signal is contained in decadal- to centennial-scale isotope variations from Antarctic ice cores?, Clim. Past, 14, 2053–2070, https://doi.org/10.5194/cp-14-2053-2018, 2018.

Münch, T. and Werner, M.: Antarctic time series of temperature, precipitation, and stable isotopes in precipitation from the ECHAM5/MPI-OM-wiso past1000 climate model simulation, v0.1.0, https://doi.org/10.5281/zenodo.4001565, 2020.

500 Münch, T., Kipfstuhl, S., Freitag, J., Meyer, H., and Laepple, T.: Regional climate signal vs. local noise: a two-dimensional view of water isotopes in Antarctic firn at Kohnen Station, Dronning Maud Land, Clim. Past, 12, 1565–1581, https://doi.org/10.5194/cp-12-1565-2016, 2016.

Münch, T., Kipfstuhl, S., Freitag, J., Meyer, H., and Laepple, T.: Constraints on post-depositional isotope modifications in East Antarctic firn from analysing temporal changes of isotope profiles, The Cryosphere, 11, 2175–2188, https://doi.org/10.5194/tc-11-2175-2017, 2017.

505 Passalacqua, O., Cavitte, M., Gagliardini, O., Gillet-Chaulet, F., Parrenin, F., Ritz, C., and Young, D.: Brief communication: Candidate sites of 1.5 Myr old ice 37 km southwest of the Dome C summit, East Antarctica, The Cryosphere, 12, 2167–2174, https://doi.org/10.5194/tc-12-2167-2018, 2018.

Persson, A., Langen, P. L., Ditlevsen, P., and Vinther, B. M.: The influence of precipitation weighting on interannual variability of stable water isotopes in Greenland, J. Geophys. Res., 116, https://doi.org/10.1029/2010JD015517, 2011.

510 Schleiss, M. and Smith, J. A.: Two Simple Metrics for Quantifying Rainfall Intermittency: The Burstiness and Memory of Interamount Times, J. Hydrometeor., 17, 421–436, https://doi.org/10.1175/JHM-D-15-0078.1, 2015.

Schlosser, E., Reijmer, C., Oerter, H., and Graf, W.: The influence of precipitation origin on the δ^{18}O–T relationship at Neumayer station, Ekströmisen, Antarctica, Ann. Glaciol., 39, 41–48, https://doi.org/10.3189/172756404781814276, 2004.

Sjolte, J., Hoffmann, G., Johnsen, S. J., Vinther, B. M., Masson-Delmotte, V., and Sturm, C.: Modeling the water isotopes in Greenland

515 precipitation 1959–2001 with the meso-scale model REMO-iso, J. Geophys. Res., 116, D18 105, https://doi.org/10.1029/2010JD015287, 2011.

Sjolte, J., Sturm, C., Adolphi, F., Vinther, B. M., Werner, M., Lohmann, G., and Muscheler, R.: Solar and volcanic forcing of North Atlantic climate inferred from a process-based reconstruction, Clim. Past, 14, 1179–1194, https://doi.org/10.5194/cp-14-1179-2018, 2018.

Sodemann, H., Masson-Delmotte, V., Schwierz, C., Vinther, B. M., and Wernli, H.: Interannual variability of Greenland winter precipi-

520 tation sources: 2. Effects of North Atlantic Oscillation variability on stable isotopes in precipitation, J. Geophys. Res., 113, D12 111, https://doi.org/10.1029/2007JD009416, _eprint: https://agupubs.onlinelibrary.wiley.com/doi/pdf/10.1029/2007JD009416, 2008.

Steig, E. J., Grootes, P. M., and Stuiver, M.: Seasonal Precipitation Timing and Ice Core Records, Science, 266, 1885–1886, https://doi.org/10.1126/science.266.5192.1885, 1994.

Stenni, B., Curran, M. A. J., Abram, N. J., Orsi, A., Goursaud, S., Masson-Delmotte, V., Neukom, R., Goosse, H., Divine, D., van Ommen,

525 T., Steig, E. J., Dixon, D. A., Thomas, E. R., Bertler, N. A. N., Isaksson, E., Ekaykin, A., Werner, M., and Frezzotti, M.: Antarctic climate variability on regional and continental scales over the last 2000 years, Clim. Past, 13, 1609–1634, https://doi.org/10.5194/cp-13-1609-2017, 2017.

Werner, M., Langebroek, P. M., Carlsen, T., Herold, M., and Lohmann, G.: Stable water isotopes in the ECHAM5 general circulation model: Toward high-resolution isotope modeling on a global scale, J. Geophys. Res., 116, D15 109, https://doi.org/10.1029/2011JD015681, 2011.

530   Werner, M., Haese, B., Xu, X., Zhang, X., Butzin, M., and Lohmann, G.: Glacial–interglacial changes in $H_2^{18}O$, HDO and deuterium excess – results from the fully coupled ECHAM5/MPI-OM Earth system model, Geosci. Model Dev., 9, 647–670, https://doi.org/10.5194/gmd-9-647-2016, 2016.